Molecular Biology of the Cell
Vol. 13, 3588–3600, October 2002

Genetic Analysis of Sorting Nexins 1 and 2 Reveals a Redundant and Essential Function in Mice

Dana Gilbert Schwarz,*† Courtney T. Griffin,* Elizabeth A. Schneider,* Della Yee,* and Terry Magnuson*‡

*Department of Genetics, University of North Carolina, Chapel Hill, North Carolina 27599; and †Department of Genetics, Case Western Reserve University School of Medicine, Cleveland, Ohio 44106

Submitted March 13, 2002; Revised June 25, 2002; Accepted July 10, 2002
Monitoring Editor: Juan Bonifacino

Sorting nexins 1 (*Snx1*) and 2 (*Snx2*) are homologues of the yeast gene *VPS5* that is required for proper endosome-to-Golgi trafficking. The prevailing thought is that Vps5p is a component of a retrograde trafficking complex called the retromer. Genetic and biochemical evidence suggest mammals may have similar complexes, but their biological role is unknown. Furthermore, if SNX1 and SNX2 belong to such complexes, it is not known whether they act together or separately. Herein, we show that mice lacking SNX1 or SNX2 are viable and fertile, whereas embryos deficient in both proteins arrest at midgestation. These results demonstrate that SNX1 and SNX2 have a highly redundant and necessary function in the mouse. The phenotype of $Snx1^{-/-};Snx2^{-/-}$ embryos is very similar to that of embryos lacking another retromer homologue, Hβ58. This finding suggests that SNX1/SNX2 and Hβ58 function in the same genetic pathway, providing additional evidence for the existence of mammalian complexes that are structurally similar to the yeast retromer. Furthermore, the viability of $Snx1^{-/-}$ and $Snx2^{-/-}$ mice demonstrates that it is not necessary for SNX1 and SNX2 to act together. Electron microscopy indicates morphological alterations of apical intracellular compartments in the $Snx1^{-/-};Snx2^{-/-}$ yolk-sac visceral endoderm, suggesting SNX1 and SNX2 may be required for proper cellular trafficking. However, tetraploid aggregation experiments suggest that yolk sac defects cannot fully account for $Snx1^{-/-};Snx2^{-/-}$ embryonic lethality. Furthermore, endocytosis of transferrin and low-density lipoprotein is unaffected in mutant primary embryonic fibroblasts, indicating that SNX1 and SNX2 are not essential for endocytosis in all cells. Although the two proteins demonstrate functional redundancy, $Snx1^{+/-};Snx2^{-/-}$ mice display abnormalities not observed in $Snx1^{-/-};Snx2^{+/-}$ mice, revealing that SNX1 and SNX2, or their genetic regulation, are not equivalent. Significantly, these studies represent the first mutations in the mammalian sorting nexin gene family and indicate that sorting nexins perform essential functions in mammals.

INTRODUCTION

A large family of cell-trafficking genes, the sorting nexins, has recently been identified. This family includes at least 15 genes in mammals, many of which have homologues in yeast (Haft *et al.*, 1998; Teasdale *et al.*, 2001). Sorting nexins 1 and 2 are homologues of the yeast vacuole protein-sorting (*VPS*) gene *VPS5*, a gene required for proper endosome-to-Golgi trafficking (Horazdovsky *et al.*, 1997; Nothwehr and Hindes, 1997). Multiple proteins depend on Vps5p for proper localization, including resident Golgi enzymes dipeptidyl amino peptidase A and Kex2p, as well as the Golgi-sorting receptor Vps10p. A type I transmembrane receptor, Vps10p binds to vacuolar hydrolases, such as carboxypeptidase Y or proteinase A, in the late Golgi and directs their sorting to the prevacuolar endosome (Marcusson *et al.*, 1994; Cooper and Stevens, 1996; Westphal *et al.*, 1996). After ligand delivery, Vps10p is transported back to the Golgi for further rounds of protein sorting. This endosome-to-Golgi recycling of Vps10p requires Vps5p. The prevailing thought is that Vps5p and four additional yeast proteins form a complex that mediates endosome-to-Golgi trafficking (Seaman *et al.*, 1998). This trafficking complex, called the retromer, seems to assemble as two subcomplexes, Vps5p/Vps17p and Vps29p/Vps35p, whose interaction is

Article published online ahead of print. Mol. Biol. Cell 10.1091/mbc.E02–03–0145. Article and publication date are at www.molbiolcell.org/cgi/doi/10.1091/mbc.E02–03–0145.

‡ Corresponding author. E-mail address: trm4@med.unc.edu.

promoted by Vps26p (Horazdovsky *et al.*, 1997; Seaman *et al.*, 1998; Reddy and Seaman, 2001). Currently, it is thought that the retromer functions as a membrane coat complex, with Vps35p selecting specific cellular cargo (Seaman *et al.*, 1998; Nothwehr *et al.*, 1999, 2000). Because Vps5p can self-assemble into spherical structures in vitro, it has been hypothesized that Vps5p may provide some of the mechanical force driving vesicular budding (Seaman *et al.*, 1998).

At least one mammalian homologue to each of the yeast retromer genes has been identified, with the exception of *VPS17*. This evolutionary conservation of the retromer homologues suggests that mammals may have trafficking complexes that are similar, at least in molecular composition, to the yeast retromer. In support of this hypothesis, it seems that the mammalian retromer homologues may interact and form multimeric complexes (Haft *et al.*, 2000). If mammals do have complexes that are structurally analogous to the yeast retromer, their exact composition and function are unclear. Because mammals lack a *VPS17* homologue needed to form a subcomplex analogous to Vps5p/Vps17p in yeast, SNX2 has been proposed to replace Vps17p in mammals, resulting in a SNX1/SNX2 heteromeric subcomplex (Haft *et al.*, 2000). However, although SNX1 and SNX2 seem to associate with one another, the proteins can also self-associate (Haft *et al.*, 2000; Kurten *et al.*, 2001). As a result, it is not known whether the two proteins act together or separately.

Notably, the recent discovery that the PX domain, present in all of the SNX proteins, binds to phosphoinositides, suggests that SNX1 and SNX2 may target assembled complexes to specific subcellular membranes (Ponting, 1996; Ago *et al.*, 2001; Bravo *et al.*, 2001; Cheever *et al.*, 2001; Ellson *et al.*, 2001; Kanai *et al.*, 2001; Xu *et al.*, 2001). Consistent with this finding, SNX1 and SNX2 are found in both cytoplasmic pools and associated with membranes (Haft *et al.*, 1998; Zhong *et al.*, 2002). Importantly, the cargo and intracellular trafficking pathways the proteins mediate are not well understood. SNX1 and SNX2 have been shown to associate with multiple cellular receptors, including epidermal growth factor receptor (EGFR), insulin receptor, platelet-derived growth factor, leptin receptor, and the thrombin receptor protease-activated receptor-1 (Kurten *et al.*, 1996; Haft *et al.*, 1998; Wang *et al.*, 2002). Although it is thought that SNX1 and SNX2 are involved in the cellular trafficking of these receptors, the exact trafficking pathway the proteins mediate is unclear. SNX1 and SNX2 seem to partially colocalize with the early endosomal antigen 1 (EEA1), suggesting a possible function in endosomal trafficking (Kurten *et al.*, 2001; Nakamura *et al.*, 2001; Teasdale *et al.*, 2001; Zhong *et al.*, 2002; Wang *et al.*, 2002).

To investigate the biology of *Snx1* and *Snx2*, we generated two targeted null mutations in the mouse, $Snx1^{tm1Mag}$ ($Snx1^{-}$) and $Snx2^{tm1Mag}$ ($Snx2^{-}$). These are the first whole animal mutations generated in the mammalian sorting nexin gene family. Our studies on $Snx1^{-/-}$, $Snx2^{-/-}$, $Snx1^{-/-}$; $Snx2^{+/-}$, $Snx1^{+/-}$;$Snx2^{-/-}$, and $Snx1^{-/-}$;$Snx2^{-/-}$ animals demonstrate that SNX1 and SNX2 have a redundant and necessary function in the mouse. We report a close similarity between the phenotype of $Snx1^{-/-}$;$Snx2^{-/-}$ embryos and embryos lacking another retromer homologue, Hβ58. Significantly, this finding indicates that these proteins act in the same genetic pathway, providing in vivo genetic evidence for the existence of mammalian complexes that are structurally similar to the yeast retromer.

MATERIALS AND METHODS

Generation of Snx1 Gene-targeted Mice

The $Snx1^{tm1Mag}$ targeting vector was generated using genomic clones obtained by screening a 129SV genomic bacterial artificial chromosome library (Research Genetics, Huntsville, AL). The nucleotide sequence of *Snx1* exon 1 was found to contain ~122 base pairs (bp) of 5′ untranslated region and 159 bp of coding sequence, corresponding to amino acids 1–53. An ~11-kilobase (kb) *Eco*RI-*Spe*I genomic fragment was cloned in a modified yeast/*Escherichia coli* shuttle vector (pRS426-BADT) that carries β-actin-diphtheria-toxin and the yeast *URA3* gene. This genomic clone (*Snx1-Eco*RI/*Spe*I-pRS426-BADT) was then used to generate a targeting vector by using yeast-based homologous recombination, described in Khrebtukova *et al.* (1998). The yeast was used to specifically replace the coding portion of exon 1 and its subsequent splice junction with an engineered *HIS3*/neomycin gene cassette. The cassette carried *HIS3* and PGK-neomycin selectable markers placed between the dual *lox*P sites of the *lox*P^2 vector (Invitrogen, Carlsbad, CA). The cassette was amplified by polymerase chain reaction (PCR) with two chimeric oligonucleotides. The first oligonucleotide contained 45 bp of *Snx1* genomic sequence corresponding to sequence upstream of the coding portion of exon 1 and 20 bp of sequence corresponding to the *lox*P^2 vector, upstream of the 5′ *lox*P site: F, 5′-GGCCCTCGCGCACCTCACACGGCTGGAGCGCTTTGCTCGCGGCAC-CCGCACGTCTAAGAAACCAT-3′. The second chimeric oligonucleotide contained 45 bp of *Snx1* genomic sequence corresponding to a portion of intron 1 and 20 bp of reverse sequence corresponding to the *lox*P^2 vector, downstream of the 3′ *lox*P site: R, 5′-CCCTTAATAAGGGTTCTCTTTTGGGGGGCTCTTTCCTGTCTGCTG-AGTGAACCTCTTCGAGGGAC-3′. The amplified cassette, now flanked on each side with *Snx1*-specific genomic sequences, was then used to transform yeast previously transformed with the *Snx1* genomic clone (*Snx1-Eco*RI/*Spe*I-pRS426-BADT), and colonies were grown under dual His^{-}/Ura^{-} selection. The resulting colonies were shuttled into bacteria, and plasmid DNA was isolated. The yeast-based replacement of the coding portion of exon 1 with the *HIS3*/neo cassette was confirmed by diagnostic restriction digests, Southern blotting, and sequencing of the excision/replacement sites. This recombined plasmid served as a complete targeting construct (Figure 1A). The *Not*I-linearized targeting vector was electroporated into mouse embryonic stem (ES) cells and cultured under G418 selection. Individual ES cell colony DNA was digested with *Spe*I, and Southern blot analysis was performed with an ~1-kb *Spe*I-EcoRI external flanking probe (Figure 1B). Thirty-two of 334 ES cell colonies revealed the correctly targeted ~5.5-kb band. Blastocysts were injected with recombinant ES cells and transferred into pseudopregnant females. Chimeric mice were bred to Black-Swiss females and germline transmission was achieved (Figure 1C). Mice were maintained on a mixed genetic background (129/Sv/Black-Swiss).

Generation of Snx2 Gene-targeted Mice

The $Snx2^{tm1Mag}$ targeting vector was generated using genomic clones obtained by screening a 129SV genomic bacterial artificial chromosome library. The *Snx2* first coding exon included 5′ untranslated region sequence and 108 bp of coding sequence, corresponding to amino acids 1–36. An ~6-kb *Snx2 Hin*dIII genomic fragment containing the first exon was cloned into the modified yeast shuttle vector pRS426-BADT (*Snx2-Hin*dIII-pRS426-BADT). Yeast homologous recombination was then used to replace the coding portion of exon one with an engineered *HIS3*/neo cassette. The cassette was PCR amplified using two chimeric oligonucleotides. The first oligonucleotide contained 45 bp of *Snx2* genomic

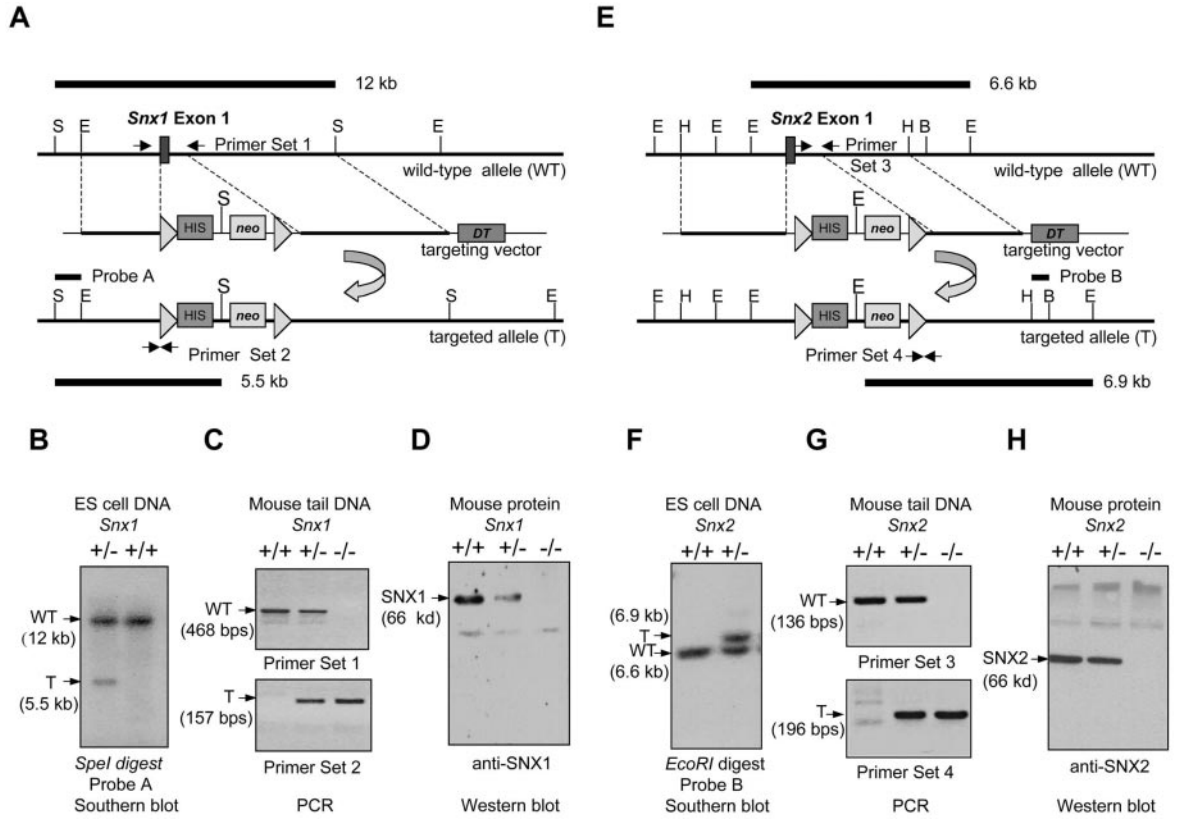

Figure 1. Gene-targeting of *Snx1* and *Snx2*. (A) Schematic representation of the exon 1 region of the wild-type *Snx1* genomic locus, the targeting construct, and the gene-targeted allele. A modified neomycin gene cassette was inserted, replacing the coding portion of exon 1. *Lox*P sites flanking the *HIS3* and neo-selectable marker genes are depicted as triangles. DT, diphtheria toxin; E, *Eco*RI; S, *Spe*I. (B) Southern blot analysis demonstrating *Snx1* homologous recombination in embryonic stem cells. Southern blots are shown using an external flanking probe (probe A) on *Spe*I digested genomic DNA isolated from two ES cell colonies transfected with the *Snx1* targeting vector. One ES cell that has undergone homologous recombination displays both the targeted (T) and wild-type alleles (WT). (C) PCR analysis of mouse tail DNA isolated from $Snx1^{+/+}$, $Snx1^{+/-}$, and $Snx1^{-/-}$ animals detecting the wild-type and targeted *Snx1* alleles. (D) Western blot analysis of SNX1 protein in lysates prepared from $Snx1^{+/+}$, $Snx1^{+/-}$, and $Snx1^{-/-}$ mice. (E) Schematic representation of the exon 1 region of the wild-type *Snx2* genomic locus, the targeting construct, and the gene-targeted allele. A modified neomycin gene cassette was inserted, replacing the coding portion of exon 1. B, *Bst*XI; H, *Hin*dIII. (F) Southern blot analysis demonstrating *Snx2* homologous recombination in ES cells. Southern blots are shown using an external flanking probe (probe B) on *Eco*RI-digested genomic DNA isolated from two ES cell lines transfected with the *Snx2* targeting construct. One ES cell that has undergone homologous recombination exhibits the targeted and wild-type alleles. (G) PCR analysis of mouse tail DNA isolated from $Snx2^{+/+}$, $Snx2^{+/-}$, and $Snx2^{-/-}$ mice detecting the wild-type and targeted *Snx2* alleles. (H) Western blot analysis of SNX2 protein in lysates prepared from $Snx2^{+/+}$, $Snx2^{+/-}$, and $Snx2^{-/-}$ mice.

sequence corresponding to sequence upstream of exon 1 and 20 bp of sequence corresponding to the *lox*P^2 vector, upstream of the 5′ *lox*P site: F, 5′-CCTTGCGTGCTCACGTGACAGGTCCGCGAGGC-CCCGGCTCTTGCA-CCGCACGTCTAAGAAACCAT-3′. The second chimeric oligonucleotide contained 45 bp of *Snx2* genomic sequence corresponding to a portion of intron 1 and 20 bp of reverse sequence corresponding to the *lox*P^2 vector, downstream of the 3′ *lox*P site: R, 5′-AGGGGAGAGGCGAGACGCACGGCGCGGGCC-TCCTCGCCGGGGGGC-AGTGAACCTCTTCGAGGGAC-3′. The amplified cassette, now flanked with *Snx2*-specific genomic sequences, was used to transform yeast previously transformed with the *Snx2* genomic clone (*Snx2-Hin*dIII-pRS426-BADT), and colonies were grown under dual His^-/Ura^- selection. The yeast-based replacement of the coding portion of the first exon with the *HIS3*/neo cassette was confirmed by diagnostic restriction digests, Southern blotting, and sequencing of the excision/replacement sites. This recombined plasmid served as a complete *Snx2* targeting vector (Figure 1E). ES cells were electroporated with *Not*I-linearized targeting vector and cultured under G418 selection. DNA isolated from individual ES cell colonies was subjected to *Eco*RI digestion and Southern blot analysis by using an ~400-base pair *Hin*dIII-*Bst*XI external flanking probe (Figure 1F). In contrast to the wild-type ~6.5-kb band, correctly targeted ES cells displayed an ~6.9-kb genomic fragment. Eight of 258 ES cell colonies screened were homologously recombined. Targeted ES cells were injected into host blastocysts and transferred into pseudopregnant females. Chimeric mice obtained were mated to Swiss-Webster females, and germline transmission was achieved (Figure 1G). Mice were maintained on a mixed genetic background.

Genotyping of Snx1 and Snx2 Alleles

Snx1. The $Snx1^{tm1Mag}$ targeted allele was detected by PCR with a forward primer designed to sequence upstream of exon 1 (5′-GGT-TCAGTGCTTGGATTGG-3′) and a reverse primer designed to *lox*P^2

vector sequence adjacent to the 5′ *lox*P site of the modified *HIS3*/neomycin gene cassette (5′-ATGGTTTCTTAGACGTGCGG-3′). The *Snx1* wild-type allele was detected by PCR with the 5′ oligonucleotide upstream of exon 1 and an intron 1 reverse primer (5′-TTCCTGATTGCTGACACCG-3′). The annealing temperature for both PCR reactions was 59°C.

Snx2. The *Snx2*^{tm1Mag} targeted allele was detected by PCR with a forward oligonucleotide (5′-GGTCCCTCGAAGAGGTTCAC-3′) designed to *lox*P[2] vector sequence adjacent to the *loxP* site at the 3′ end of the engineered gene cassette and a reverse oligonucleotide (5′-GTCACAGGTGTCACCCGAC-3′) designed to sequence within intron 1. The *Snx2* wild-type allele was detected using a forward primer designed within exon 1 (5′-ACGTGAAGCCCACAGACTTT-3′) and the reverse primer within intron 1, described above. The annealing temperature for both PCR reactions was 61°C.

Generation of Antibodies and Western Blots

Rabbit antibodies were raised to mouse SNX1 amino acid sequences KNGSKENGIHEDQDQEPQ and SHSPQEATNSPKPQPSYE and to mouse SNX2 sequences SANSNGSKPVEVVLDDDRE and STLESSPSSPEPAS and were serum affinity purified (Zymed Laboratories, South San Francisco, CA). Antisera were used at dilutions between 1:250 and 1:500. Lysates were made from whole mouse brains in 1% SDS, 50 mM Tris, pH 7.5, with Complete protease inhibitors (Roche Applied Science, Indianapolis, IN). Western blots were conducted as described in Harlow and Lane (1999).

Tetraploid Aggregations

B6;129S-*Gtros*a26 homozygous mice (Jackson Laboratories, Bar Harbor, ME) were mated to superovulated *Snx1*$^{+/+}$;*Snx2*$^{+/+}$ CD-1 females. Embryos were harvested from the oviducts at E1.5. The blastomeres of the two-cell stage embryos were electrofused using a CF-150B impulse generator (Biological Laboratory Equipment, Budapest, Hungary), according to the manufacturer's instructions, to produce tetraploid embryos. The embryos were then cultured in KSOM media under mineral oil at 37°C, 5% CO_2 until aggregation. *Snx1*$^{-/-}$;*Snx2*$^{+/-}$ males were mated to superovulated *Snx1*$^{-/-}$;*Snx2*$^{+/-}$ females, and the embryos were harvested at E2.5. The zona pellucida from both tetraploid and diploid embryos was removed with acidic Tyrode's solution. One tetraploid and one diploid embryo were aggregated at the eight-cell stage, as described previously (Nagy *et al.*, 1990, 1993). The resulting chimeric embryos were cultured until blastocyst stage and were transferred into the uterine horns of pseudopregnant females. The chimeric embryos were recovered at E12.5 and subjected to whole-mount X-gal staining as described in Hogan *et al.* (1994). Each embryo's yolk sac was pierced before staining to allow tissue penetration of the solutions. After staining, each chimeric embryo was photographed and then dissected. Three separate samples of embryonic tissue (usually the tail and the two limb buds) were removed and genotyped by PCR.

Southern Blotting

Total DNA extracted from cells was digested with the appropriate restriction enzymes, separated on a 0.8% agarose gel, transferred to nylon membranes, and hybridized at 42°C overnight with a random-prime–labeled probe with [^{32}P]dCTP (Amersham Biosciences, Piscataway, NJ). Membranes were washed in 2× SSC, 0.1% SDS, 5 min at 25°C; in 0.2× SSC, 0.1% SDS, 30 min at 25°C; and in 0.2× SSC, 0.1% SDS, ~1 h at 40–50°C.

Embryonic Histology

Snx1$^{-/-}$;*Snx2*$^{+/-}$ mice were intercrossed. Noon of the day vaginal plugs were detected was considered embryonic day 0.5. At the appropriate embryonic day, decidua were removed from the uterus and fixed in either 4% paraformaldehyde or Bouin's fixative overnight at 4°C. Samples were embedded in paraffin, sectioned, and stained with hematoxylin and eosin.

Electron Microscopy

Five *Snx1*$^{-/-}$;*Snx2*$^{-/-}$ embryos were dissected and fixed (2% paraformaldehyde, 2.5% glutaraldehyde, 0.1 M sodium cacodylate, pH 7.4) along with the yolk sac and placental tissues at E9.5. Four stage-matched wild-type embryos (E8.5) of similar genetic background served as controls. Tissues were embedded and sectioned in standard manner. The proximal, columnar portion of the yolk sac was then analyzed.

Fluorescence Microscopy

Snx1$^{-/-}$;*Snx2*$^{-/-}$ embryos were harvested with the yolk sac and placental tissues intact, along with normal littermate controls. For live cell staining, the embryos were cultured (37°C, 5% CO_2) in 60 nM LysoTracker Red (Molecular Probes, Eugene, OR) in α minimal essential medium (αMEM) (Invitrogen) with 15% embryonic stem cell-qualified fetal bovine serum (Invitrogen). Embryos were cultured ~1–1.5 h in the dark. The columnar portion of the yolk sac was isolated and rinsed with KSOM media. The yolk sac was placed onto a glass slide in a drop of KSOM, a coverslip was added, and the cells were imaged immediately. For immunostaining, harvested yolk sacs were fixed in 4% paraformaldehyde for 5 min on ice, permeabilized in methanol for 30 s, and rinsed with phosphate-buffered saline (PBS). Yolk sacs were washed three times (5 min each) in 1% nonfat dried milk and 150 mM sodium acetate, ~pH 7, in PBS. Yolk sacs were blocked three times in 1% nonfat dried milk in PBS and then were incubated with the appropriate primary antibodies for 1 h at 25°C. Rabbit anti-early endosomal antigen 1 antibody (Affinity Bioreagents, Golden, CO), rat anti-lysosome–associated membrane protein-1 antibody (BD Biosciences, San Jose, CA), and rat anti-lysosome–associated membrane protein-2 antibody (BD Biosciences) were used. Yolk sacs were then washed and incubated with the appropriate species-specific AlexaFluor 488-conjugated secondary antibodies (Molecular Probes) for 1 h at 25°C in the dark. Yolk sacs were subsequently washed five times with PBS and were imaged.

Endocytic Uptake Assays and Confocal Microscopy

To generate primary embryonic fibroblasts, E9.5 embryos from wild-type or *Snx1*$^{-/-}$;*Snx2*$^{+/-}$ crosses were dissected into αMEM. Individual embryos were passed through a 22-gauge needle and plated into 12-well tissue culture dishes coated with 0.1% gelatin. Fibroblasts growing out of the minced embryos were cultured, trypsinized, and expanded into larger tissue culture dishes three times to generate a sufficient number of cells for three separate uptake assays. Fibroblasts were cultured and maintained in αMEM supplemented with 15% embryonic stem cell-qualified fetal bovine serum, penicillin (100 U/ml), and streptomycin (100 μg/ml) (Invitrogen) and were genotyped by PCR before use in experiments.

Primary embryonic fibroblasts were plated on gelatin-coated glass coverslips (22 × 22 mm) in six-well dishes and were grown overnight. For LysoTracker Red staining, fibroblasts were incubated with 60 nM of the dye for 90 min at 37°C, 5% CO_2. Coverslips were subsequently rinsed in PBS, mounted on glass slides without the addition of mounting media, and analyzed by confocal microscopy as described previously (Wang *et al.*, 2002). For transferrin and low-density lipoprotein (LDL) uptake assays, fibroblasts were serum starved in αMEM supplemented with 0.1% bovine serum albumin for 100 min and were subsequently incubated for 15 min with 50 μg/ml human transferrin labeled with AlexaFluor 594 (Molecular Probes) or for 40 min with 10 μg/ml human LDL labeled with BODIPY FL fluorophore (Molecular Probes) at 37°C, 5% CO_2, respectively. After uptake, cells were washed three times for 5 min each in PBS/1% bovine serum albumin on ice and were fixed for 5

Table 1. Genotypes of offspring from $Snx1^{+/-}$; $Snx2^{+/-}$ intercrosses

Snx1 genotype	*Snx2* genotype	Offspring no.	Percentage	% Expected
+/−	+/−	55	30.4	25
−/−	+/−	28	15.5	12.5
+/+	+/−	27	14.9	12.5
+/−	+/+	26	14.4	12.5
+/−	−/−	15	8.3	12.5
+/+	+/+	11	6.1	6.25
+/+	−/−	10	5.5	6.25
−/−	+/+	9	5.0	6.25
−/−	−/−	0	0	6.25

min with 4% paraformaldehyde on ice. Coverslips were mounted on glass slides with FluorSave Reagent (Calbiochem, San Diego, CA) and were analyzed by confocal microscopy as described previously (Wang *et al.*, 2002).

RESULTS

Generation of Mice Lacking SNX1

To study the genetics of *Snx1*, a targeted mutation was generated in the mouse by using homologous recombination. The targeting vector was engineered to remove the coding portion of the first exon, as well as the subsequent splice junction (Figure 1A). Homologously recombined ES cells were obtained, chimeric mice were generated, and germline transmission was achieved (Figure 1, B and C). $Snx1^{+/-}$ intercrosses revealed that $Snx1^{-/-}$ progeny were born in expected Mendelian ratios: 36 $Snx1^{+/+}$, 60 $Snx1^{+/-}$, and 38 $Snx1^{-/-}$. Subsequent matings determined that both male and female $Snx1^{-/-}$ mice were fertile. Histological and hematological analysis of the $Snx1^{-/-}$ mice failed to identify any defects (our unpublished data). In addition, $Snx1^{-/-}$ animals were aged for 14 mo without any apparent abnormalities. To determine whether the targeted mutation resulted in a genetic null, antibodies were raised to specific SNX1 amino acid sequences. Importantly, to avoid antibody cross-reactivity the chosen amino acid stretches were significantly divergent between SNX1 and SNX2. The purified antibodies were used to perform Western blot analysis on tissue lysates prepared from wild-type, heterozygous, and homozygous animals. As expected, lysates from wild-type mice exhibited an ~66-kDa band corresponding to the known molecular mass of SNX1. Lysates from *Snx1* heterozygous mice had an ~66-kDa band of reduced intensity, whereas no band was detected in lysates from the homozygous animals (Figure 1D). Importantly, no additional bands appeared in lysates from the *Snx1* homozygous mice, demonstrating no truncated protein products were produced. Thus, the targeted mutation $Snx1^{tm1Mag}$ is a null allele, resulting in a complete absence of SNX1 protein. This result also demonstrates that the SNX1 antisera did not cross-react with SNX2. This null allele represents the first mutation generated in the mammalian sorting nexin gene family. These results reveal that SNX1 is not required for mouse viability or fertility. Due to evolutionary homology between SNX1 and SNX2 (~60% of amino acids are identical), the lack of an overt phenotype in the null mice could be due to functional redundancy between the proteins. Therefore, we sought to generate a second null mutation, this time in *Snx2*.

Generation of Mice Lacking SNX2

To generate the *Snx2* targeted mutation, a targeting vector was engineered lacking the coding portion of the first exon and its subsequent splice junction (Figure 1E). Homologous recombination in ES cells was achieved (Figure 1F). These genetically altered ES cells were used to generate chimeric animals, and germline transmission of the targeted mutation was realized (Figure 1G). Intercrosses of $Snx2^{+/-}$ animals produced $Snx2^{-/-}$ offspring in expected Mendelian ratios: 32 $Snx2^{+/+}$, 62 $Snx2^{+/-}$, and 33 $Snx2^{-/-}$. In addition, $Snx2^{-/-}$ animals were fertile and were aged for 10 mo without displaying overt abnormalities. Antibodies raised to SNX2-specific amino acid sequences were used to perform Western blot analysis on tissue lysates prepared from $Snx2^{+/+}$, $Snx2^{+/-}$, and $Snx2^{-/-}$ animals. Lysates from the $Snx2^{+/+}$ mice displayed a single band at ~66 kDa, corresponding to the known molecular mass of SNX2. The band was reduced in intensity in lysates from $Snx2^{+/-}$ mice, and no bands were present in lysates from the $Snx2^{-/-}$ animals (Figure 1H). These results show that the targeted mutation $Snx2^{tm1Mag}$ is a null allele and that SNX2, like SNX1, is not required for mouse viability or fertility.

Mouse Development Requires Either SNX1 or SNX2

To determine whether the lack of an overt phenotype in the $Snx1^{-/-}$ and $Snx2^{-/-}$ animals was due to functional redundancy between SNX1 and SNX2, we attempted to generate $Snx1^{-/-}$;$Snx2^{-/-}$ mice by intercrossing $Snx1^{+/-}$;$Snx2^{+/-}$ animals (Table 1). However, no $Snx1^{-/-}$;$Snx2^{-/-}$ animals were obtained out of 181 offspring ($P < 0.001$), indicating $Snx1^{-/-}$;$Snx2^{-/-}$ embryos do not survive to term. These results demonstrate that the presence of either SNX1 or SNX2 is required for mouse development.

$Snx1^{-/-}$;$Snx2^{-/-}$ Embryos Arrest at Midgestation

To determine the timing of embryonic lethality, timed matings and embryonic dissections were carried out (Table 2). We found that $Snx1^{-/-}$;$Snx2^{-/-}$ embryos typically arrest between embryonic day 9.5 (E9.5) and 11.5. Histological analysis revealed that $Snx1^{-/-}$;$Snx2^{-/-}$ embryos are retarded in growth by E7.5 (Figure 2, A and B). At E8.5, the mutant embryos exhibited disproportionate growth of the

Table 2. Numbers of live embryos from *Snx1*$^{-/-}$; *Snx2*$^{+/-}$ intercrosses

Embryonic day	*Snx1*$^{-/-}$; *Snx2*$^{+/+}$	*Snx1*$^{-/-}$; *Snx2*$^{+/-}$	*Snx1*$^{-/-}$; *Snx2*$^{-/-}$	Resorptions
E8.5	18	40	18	0
E9.5	20	42	24	1
E10.5	21	43	12	8
E11.5	28	46	1	24
E12.5	17	45	0	26

extraembryonic structures compared with the embryonic ectoderm (Figure 2C). Most mutant embryos developed head-folds, heart, somites, and neural folds that had not fused (Figure 2, D–G). In addition, embryos were usually truncated at the posterior end, exhibited variability in chorioallantoic fusion, and in most cases, did not undergo axial rotation (Figure 2E). These results demonstrate that early embryogenesis requires the function of SNX1 or SNX2. No-

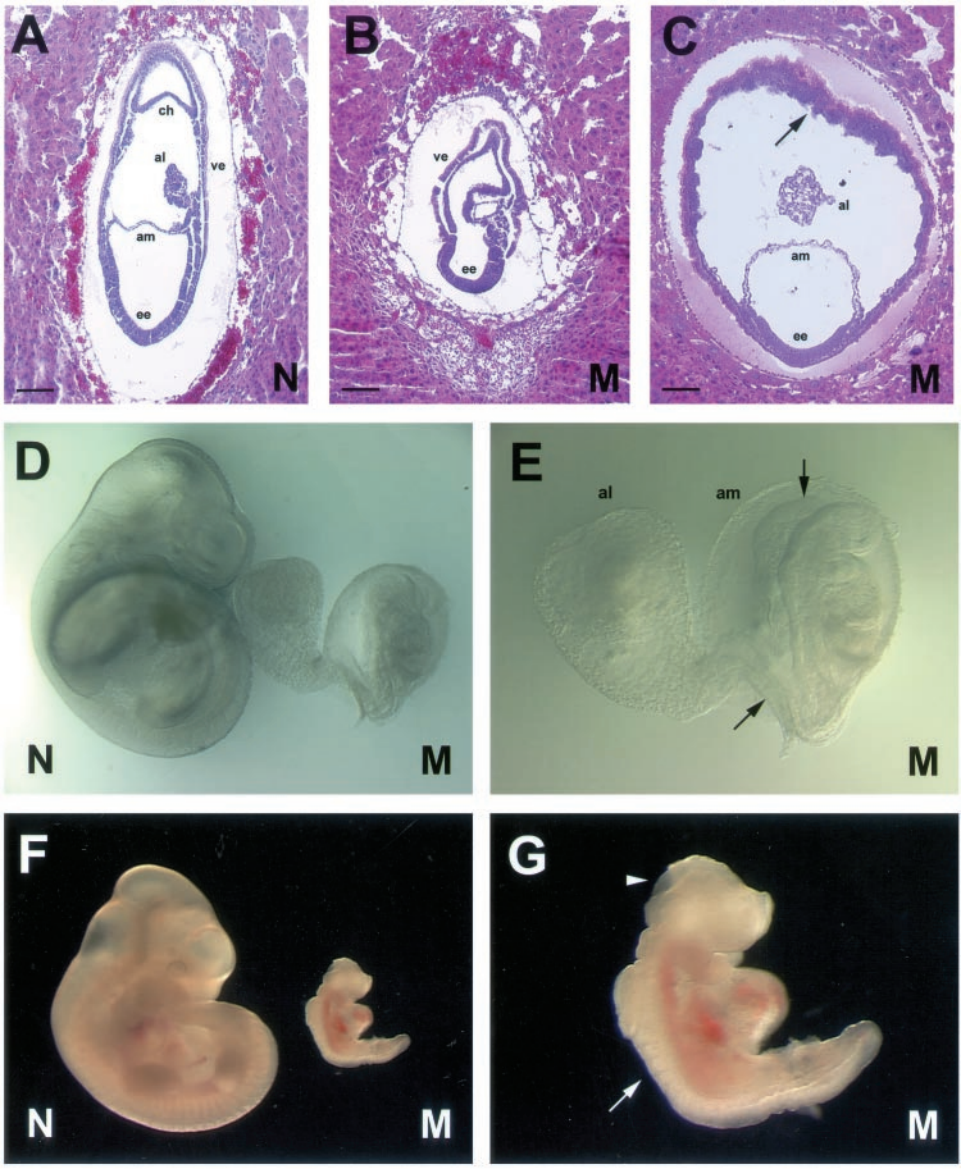

Figure 2. Phenotypic analysis of *Snx1*$^{-/-}$;*Snx2*$^{-/-}$ embryos. (A and B) Histological analysis of mutant (M, *Snx1*$^{-/-}$;*Snx2*$^{-/-}$) and normal (N) littermate controls at E7.5. Sagittal paraffin sections stained with hematoxylin and eosin (H&E) are shown. The embryonic ectoderm (ee), chorion (ch), amnion (am), allantois (al), and visceral endoderm (ve) of the yolk sac are labeled. Black bars, ~100 μm. Note that the mutants are significantly smaller and already delayed in development. (C) Histological section from an E8.5 mutant embryo, demonstrating the overgrowth of the yolk sac (arrow) and the disproportionate growth of the extraembryonic structures compared with the embryonic ectoderm. Black bars, ~100 μm. (D and E) Photographs of normal (left) and mutant (right) embryos at E9.5. The mutant embryo (shown in closeup in E) displays developmental delay, a large allantois, a truncated posterior (arrow), and neural folds (arrowhead) that have not fused. (F and G) Photographs of normal (left) and mutant (right) embryos at E10.5, showing the most advanced stage reached by *Snx1*$^{-/-}$; *Snx2*$^{-/-}$ embryos. The mutant embryo (shown in closeup in G), displays developmental delay, somites (arrow), heart tissue, and neural folds (arrowhead) that have not fused.

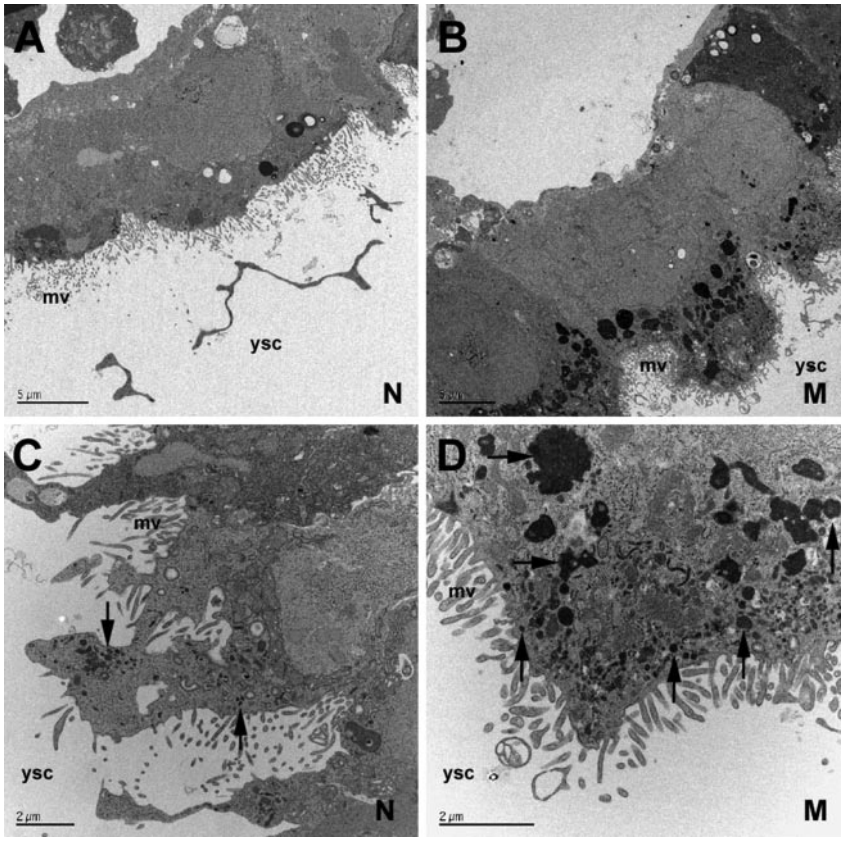

Figure 3. Electron microscopy of $Snx1^{-/-}$;$Snx2^{-/-}$ yolk-sac visceral endoderm. (A and B) Electron microscopy of normal control (N, $Snx1^{+/+}$;$Snx2^{+/+}$) and mutant (M, $Snx1^{-/-}$;$Snx2^{-/-}$) visceral endoderm. The apical microvilli (mv) and yolk-sac cavity (ysc) are labeled. (C and D) Wild-type and mutant apical visceral endoderm at higher magnification. Numerous apical electron dense compartments (arrows) are seen in the mutant images.

tably, these embryos display a phenotype closely resembling that of embryos lacking another retromer homologue, Hβ58 (Radice *et al.*, 1991).

Abnormal Morphology in Apical Visceral Endoderm

The conclusion from previous studies on Hβ58-deficient embryos was that the embryonic lethality could be due to defects in the yolk-sac visceral endoderm (Lee *et al.*, 1992). In humans and mice, before the development of the chorioallantoic placenta, the yolk-sac visceral endoderm provides the developing embryo with the necessary nutrient supply (Jollie, 1990). As a result, embryos carrying mutations that cause abnormal yolk sac development often arrest at developmental stages comparable with the arrest of $Snx1^{-/-}$;$Snx2^{-/-}$ and $H\beta58^{-/-}$ embryos. Given that one of the earliest defects observed in the Hβ58-deficient embryos is growth retardation of the embryonic ectoderm and that Hβ58 is highly expressed in the visceral endoderm, it was hypothesized that disruptions in nutrient or growth factor delivery could be responsible for the early embryonic phenotype (Radice *et al.*, 1991; Lee *et al.*, 1992). Because embryos lacking SNX1 and SNX2 display a similar phenotype, we investigated whether the visceral endoderm cells of $Snx1^{-/-}$; $Snx2^{-/-}$ yolk sacs display morphological abnormalities. To analyze $Snx1^{-/-}$;$Snx2^{-/-}$ visceral endoderm morphology we performed electron microscopy on yolk sacs from E9.5 mutant embryos and stage-matched wild-type controls. The analysis revealed an increased prevalence of apical electron dense structures in the yolk-sac visceral endoderm of $Snx1^{-/-}$;$Snx2^{-/-}$ embryos compared with wild-type embryos (Figure 3).

LysoTracker Red, a fluorescent dye that selectively accumulates in acidic organelles, was used to further characterize the morphology of $Snx1^{-/-}$;$Snx2^{-/-}$ visceral endoderm cells. Five E9.5 $Snx1^{-/-}$;$Snx2^{-/-}$ embryos were harvested, keeping the visceral endoderm of the yolk sac and the placental tissues intact, along with five normal littermate controls. After culturing the embryos in media containing the fluorescent dye, the proximal portion of the yolk sac was removed and analyzed by fluorescence microscopy. The fluorescent staining pattern in the $Snx1^{-/-}$;$Snx2^{-/-}$ yolk-sac visceral endoderm seemed to be altered compared with normal littermate controls. Although the control visceral endoderm cells exhibited a more uniform pattern of fluorescence (Figure 4, A and C), the $Snx1^{-/-}$;$Snx2^{-/-}$ embryos displayed a more punctate fluorescence pattern (Figure 4, B and D). Similarly, five E8.5 $Snx1^{-/-}$;$Snx2^{-/-}$ embryos were analyzed along with eight normal littermate controls. The $Snx1^{-/-}$;$Snx2^{-/-}$ visceral endoderm cells also exhibited a more punctate fluorescence pattern compared with normal littermate controls (our unpublished data).

To further define the punctate structures detected by LysoTracker Red staining of $Snx1^{-/-}$;$Snx2^{-/-}$ visceral endoderm cells, we immunostained mutant and control yolk sacs with various antibodies against subcellular marker proteins. First, we assessed the morphology of mature lyso-

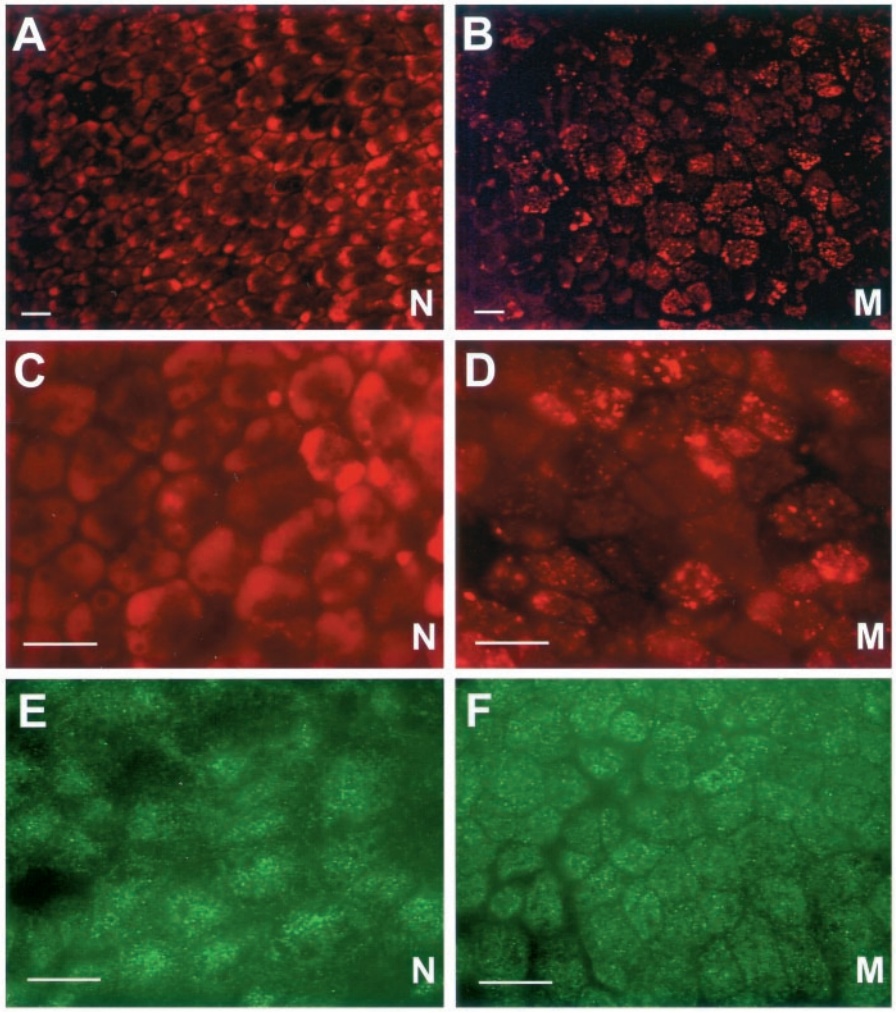

Figure 4. Fluorescence microscopy of the yolk-sac visceral endoderm. (A and B) Fluorescence pattern of acidic LysoTracker-positive compartments (stained in red) is shown in normal (N) littermate control and mutant (M, *Snx1*$^{-/-}$;*Snx2*$^{-/-}$) visceral endoderm. Note that the mutant visceral endoderm cells have a less uniform and more punctate staining pattern compared with the normal controls. (C and D) Fluorescence staining pattern of acidic LysoTracker-positive compartments is shown at higher magnification. (E and F) Immunostaining pattern of EEA1 in the normal and mutant littermates is shown. Bars, 20 μm.

somes by immunostaining yolk sacs with antibodies to lysosomal proteins LAMP1 and LAMP2. We did not detect an altered staining pattern between control and mutant yolk-sac visceral endoderm (our unpublished data). Likewise, to visualize the morphology of early endosomes, immunostaining of early endosomal marker protein EEA1 was performed. The EEA1 immunostaining did not reveal significant differences between the *Snx1*$^{-/-}$;*Snx2*$^{-/-}$ and the control visceral endoderm (Figure 4, E and F). We therefore conclude that the LysoTracker-positive structures in the *Snx1*$^{-/-}$;*Snx2*$^{-/-}$ visceral endoderm cells do not seem to be either early endosomes or mature lysosomes.

Tetraploid Aggregations Suggest Defects in Extraembryonic and Embryonic Tissues

Defects in visceral endoderm trafficking could be the underlying cause of the *Snx1*$^{-/-}$;*Snx2*$^{-/-}$ embryonic lethality. To address whether defects in extraembryonic tissues are the cause of the embryonic arrest, we performed tetraploid aggregation rescue experiments (Nagy *et al.*, 1993). These experiments take advantage of the fact that tetraploid cells in a diploid/tetraploid chimeric embryo only contribute to extraembryonic tissues. As a result, we can use diploid/tetraploid chimeras to generate *Snx1*$^{-/-}$;*Snx2*$^{-/-}$ embryos that develop with partially wild-type extraembryonic tissues.

As a marker for wild-type cells we took advantage of mice harboring the ROSA26 gene-trap retroviral integration that contains a *lac*Z reporter sequence expressed ubiquitously. As a result, ROSA26 can be stained with X-gal (blue) and used to monitor the presence of these cells. ROSA26 homozygous animals were mated with wild-type females, and embryos were harvested. Wild-type embryos carrying ROSA26 were subjected to electrofusion to generate tetraploid embryos. Diploid embryos were harvested from *Snx1*$^{-/-}$;*Snx2*$^{+/-}$ intercrosses and were aggregated with the ROSA26 tetraploid embryos. These aggregated embryos were transferred at the blastocyst stage to pseudopregnant females. The resulting chimeras were dissected at E12.5 with the placental tissues and the visceral endoderm of the yolk sac intact, fixed briefly, and subjected to X-gal staining (Figure 5A). After photographing the yolk sacs of each embryo, embryonic tissues

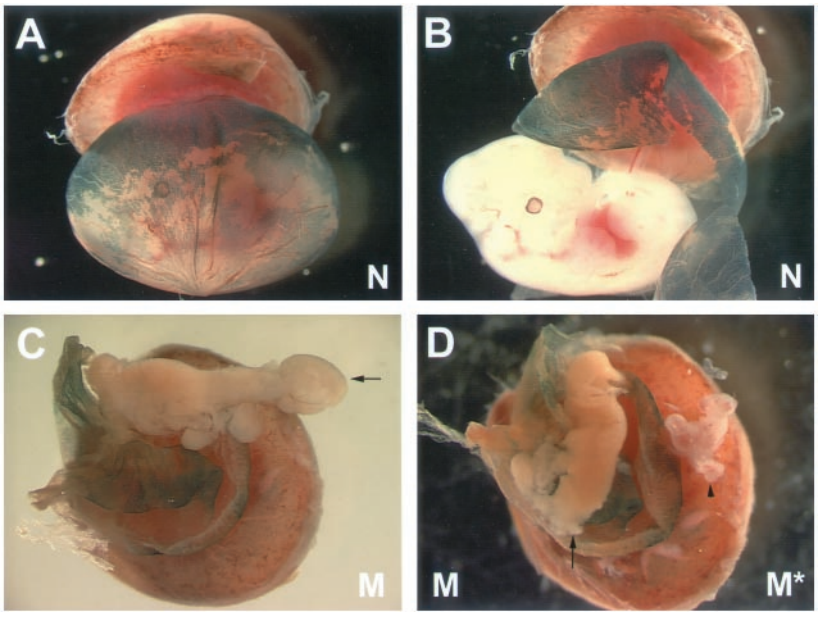

Figure 5. Tetraploid aggregations. (A and B) Photographs of an E12.5 normal littermate control (N) embryo with whole-mount X-gal staining (blue) marking the wild-type tetraploid cells contributing to the visceral endoderm of the yolk sac. There are no tetraploid cells seen contributing to the embryo proper (B). (C) Photographs of an E12.5 mutant (M, $Snx1^{-/-};Snx2^{-/-}$) embryo with whole-mount X-gal staining marking the wild-type tetraploid cells contributing to the visceral endoderm of the yolk sac. Note that this embryo has already arrested. An abnormal tail region is seen (arrow). (D) On the left is the mutant embryo (M, $Snx1^{-/-};Snx2^{-/-}$, arrow) seen in C (a portion of the abnormal tail has been removed for genotyping). On the right is a mutant embryo (M*, $Snx1^{-/-};Snx2^{-/-}$) obtained by natural matings. This embryo is representative of the most well-developed stage mutants typically achieve (arrowhead).

were dissected and genotyped in triplicate. As expected, none of the chimeras exhibited X-gal staining in the embryo proper (Figure 5B). Approximately 50% of the dissected embryos displayed some degree of X-gal staining in the extraembryonic tissues. Despite the generation of embryos with significant wild-type contribution to the yolk-sac visceral endoderm, we did not completely rescue $Snx1^{-/-};Snx2^{-/-}$ embryonic lethality. However, one $Snx1^{-/-};Snx2^{-/-}$ embryo with wild-type contribution to the yolk-sac visceral endoderm did achieve a much larger developmental size than any of the mutants generated from $Snx1^{-/-};Snx2^{+/-}$ intercrosses (Figure 5, C and D). Despite this larger size, this mutant embryo still arrested by the time of dissection (E12.5). The larger development of this mutant embryo suggests that defects exist in the extraembryonic tissues that are being corrected by the presence of wild-type cells. However, the failure to rescue lethality indicates that defects may also be present in the embryonic tissues.

Morphology and Endocytosis Are Normal in Primary Embryonic Fibroblasts

To determine whether the abnormalities observed in mutant extraembryonic visceral endoderm cells were recapitulated in embryonic cells, we generated primary fibroblasts from wild-type and $Snx1^{-/-};Snx2^{-/-}$ embryos. The fibroblasts were analyzed for LysoTracker Red accumulation (Figure 6, A and B). Dye accumulation was indistinguishable in wild-type vs. mutant cells, indicating that acidic organelles are not enlarged in mutant embryonic fibroblasts as they were in mutant visceral endoderm cells. To assess the viability of endocytic processing in $Snx1^{-/-};Snx2^{-/-}$ fibroblasts, cells were incubated in the presence of fluorescent transferrin or fluorescent LDL to allow receptor-mediated uptake and trafficking of the labeled proteins (Figure 6, C–F). On uptake, transferrin and its receptor are sorted to recycling endosomes that deliver the complex back to the plasma membrane, whereas LDL dissociates from its receptor after internalization and traffics to lysosomes (Mayor *et al.*, 1993). Fluorescently labeled transferrin accumulated comparably in small, punctate structures throughout wild-type and $Snx1^{-/-};Snx2^{-/-}$ fibroblasts. Transferrin-positive vesicles were predominantly observed in perinuclear regions, which are known sites of recycling endosome localization. Likewise, fluorescent LDL accumulation was indistinguishable in wild-type vs. mutant fibroblasts. LDL accumulated in small, punctate structures throughout the cells and more prevalently in larger, punctate structures, presumably late endosomes or lysosomes. These results demonstrate that endocytosis of transferrin and LDL is not compromised by the absence of SNX1 and SNX2.

Approximately 40% of $Snx1^{+/-};Snx2^{-/-}$ Embryos Do Not Survive Development

$Snx1^{+/-};Snx2^{+/-}$ intercrosses indicated that $Snx1^{+/-};Snx2^{-/-}$ mice were underrepresented (Table 1). We recovered 15 progeny vs. the ~24 expected. This result is in contrast to $Snx1^{-/-};Snx2^{+/-}$ mice, which were present in expected numbers; 28 progeny were recovered vs. the ~24 expected. To confirm these results, $Snx1^{+/+};Snx2^{-/-}$ mice were mated to $Snx1^{+/-};Snx2^{-/-}$ mice, and all offspring were genotyped. Although this cross should yield equal numbers of $Snx1^{+/+};Snx2^{-/-}$ and $Snx1^{+/-};Snx2^{-/-}$ offspring, 116 of the former vs. 71 of the latter were recovered. These results demonstrate that $Snx1^{+/-};Snx2^{-/-}$ mice are under-represented ($P < 0.01$) and suggest that ~40% of $Snx1^{+/-};Snx2^{-/-}$ embryos do not survive development.

$Snx1^{+/-};Snx2^{-/-}$ Mice are Born Runted Due to Developmental Growth Retardation

The $Snx1^{+/-};Snx2^{-/-}$ offspring that survived development seemed to be runted. To determine the degree of runting and its progression, $Snx1^{+/-};Snx2^{-/-}$ mice were crossed

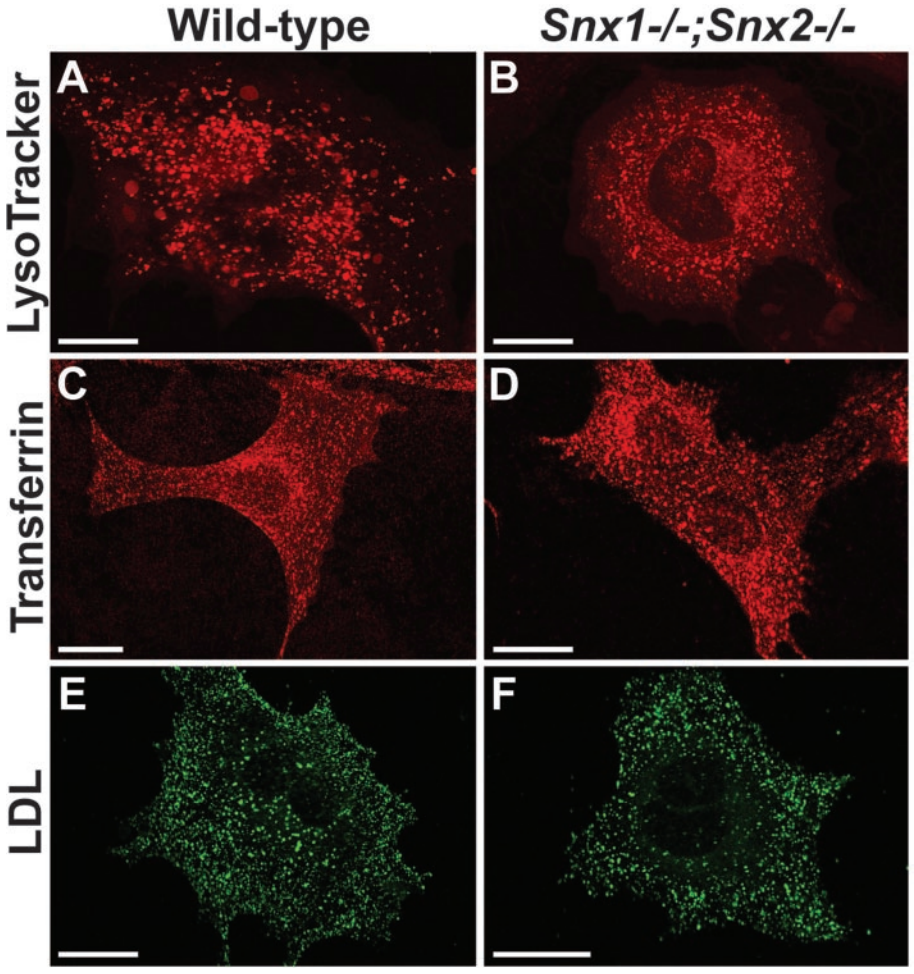

Figure 6. Confocal microscopy of primary embryonic fibroblasts. (A and B) Fluorescence pattern of acidic LysoTracker Red-positive compartments is shown in wild-type (A) and $Snx1^{-/-}$; $Snx2^{-/-}$ (B) primary embryonic fibroblasts. (C and D) Distribution of fluorescent transferrin is shown in wild-type (C) and $Snx1^{-/-}$; $Snx2^{-/-}$ (D) fibroblasts after 15 min of endocytic uptake. (E and F) Distribution of fluorescent LDL is shown in wild-type (E) and $Snx1^{-/-}$; $Snx2^{-/-}$ (F) fibroblasts after 40 min of endocytic uptake. Bars, 20 μm.

with $Snx1^{+/+}$;$Snx2^{-/-}$ mice, and all offspring were weighed and genotyped (Figure 7A). At birth, $Snx1^{+/-}$;$Snx2^{-/-}$ mice were ~20% smaller than $Snx1^{+/+}$;$Snx2^{-/-}$ littermates, 1.20 ± 0.04 g vs. 1.48 ± 0.04 g ($P < 0.001$). This runting continued into adulthood with the $Snx1^{+/-}$;$Snx2^{-/-}$ mice remaining ~10–20% smaller than $Snx1^{+/+}$;$Snx2^{-/-}$ littermates (Figure 7A). Moreover, $Snx1^{+/-}$;$Snx2^{-/-}$ mice are fertile. To determine whether the runting was due to growth retardation in development, timed matings and embryonic dissections were carried out. At E15.5, all embryos were dissected and weighed. The $Snx1^{+/-}$;$Snx2^{-/-}$ embryos weighed less than $Snx1^{+/+}$;$Snx2^{-/-}$ littermates, 0.47 g ± 0.02 g vs. 0.56 ± 0.02 g ($P < 0.01$). These results indicate that the runting of $Snx1^{+/-}$;$Snx2^{-/-}$ mice is embryonic in origin. Further embryonic dissections were performed at E11.5. All embryos were photographed and measured for size. The analysis suggested that $Snx1^{+/-}$;$Snx2^{-/-}$ embryos were smaller by E11.5 (Figure 7, B and C).

SNX1 and SNX2, or Their Genetic Regulation, Are Not Equivalent

In contrast to the ~40% embryonic lethality and runting of $Snx1^{+/-}$;$Snx2^{-/-}$ mice, crosses between $Snx1^{-/-}$;$Snx2^{+/+}$ and $Snx1^{-/-}$;$Snx2^{+/-}$ mice yielded 108 $Snx1^{-/-}$;$Snx2^{+/+}$ vs. 110 $Snx1^{-/-}$;$Snx2^{+/-}$ offspring. These results indicate $Snx1^{-/-}$; $Snx2^{+/-}$ mice are born in expected Mendelian ratios. Additionally, there were no significant weight differences between $Snx1^{-/-}$;$Snx2^{+/+}$ and $Snx1^{-/-}$;$Snx2^{+/-}$ mice (day 7: 5.2 ± 0.1 g vs. 5.1 ± 0.1 g, day 14: 8.4 ± 0.2 g vs. 8.4 ± 0.2 g, day 21: 12.8 ± 0.3 g vs. 12.9 ± 0.5 g). These findings cannot be readily explained by genetic background differences and therefore represent the first in vivo evidence that *SNX1* and *SNX2*, or their genetic regulation, are not equivalent.

Genetic Interaction with EGFR Mutation Waved-2

SNX1 is thought to be involved in EGFR trafficking (Kurten *et al.*, 1996). Therefore, to genetically address whether SNX1 affects EGFR function in vivo, we crossed mice harboring the EGFR hypomorphic mutation waved-2 ($EGFR^{Wa-2}$) and mice carrying the *Snx1* targeted mutation. Genetic interactions have been previously shown between the waved-2 mutation and other genes that interact with EGFR (Chen *et al.*, 2000). Mice homozygous for the waved-2 mutation exhibit both wavy whiskers and fur and demonstrate lactation defects (Luetteke *et al.*, 1994; Fowler *et al.*, 1995). The EGFR point

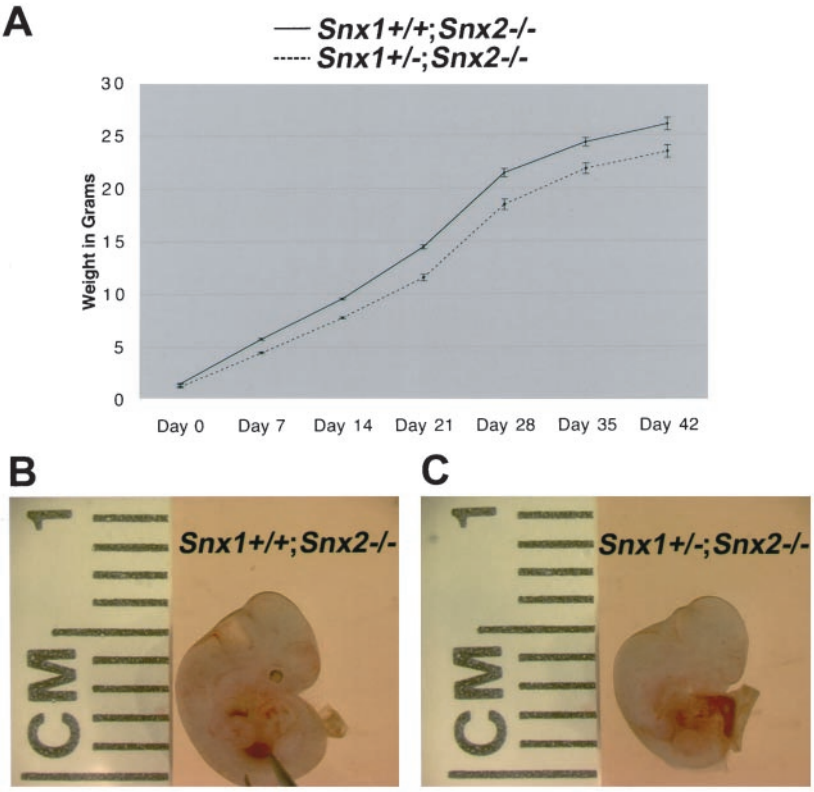

Figure 7. Growth retardation of $Snx1^{+/-}$;$Snx2^{-/-}$ mice. (A) Weights of $Snx1^{+/-}$;$Snx2^{-/-}$ and $Snx1^{+/+}$; $Snx2^{-/-}$ littermate controls from postnatal day 0 to day 42. (B) Photograph of a typical $Snx1^{+/+}$;$Snx2^{-/-}$ embryo at E11.5. (C) Photograph of a typical $Snx1^{+/-}$;$Snx2^{-/-}$ embryo at E11.5. Note the smaller size of this embryo compared with the one in B.

mutation, resulting in a valine-to-glycine substitution at residue 743, causes the receptor kinase activity to be reduced to 10–20% of normal (Luetteke *et al.*, 1994). We generated mice heterozygous for both the waved-2 and the *Snx1* mutations, and these mice were intercrossed. The crosses revealed that 15 of the 193 offspring were $EGFR^{Wa\text{-}2/Wa\text{-}2}$;$Snx1^{-/-}$, indicating $EGFR^{Wa\text{-}2/Wa\text{-}2}$;$Snx1^{-/-}$ mice are born in expected Mendelian ratios. In addition, the phenotype of the mice remained the same as that of $EGFR^{Wa\text{-}2/Wa\text{-}2}$ animals, demonstrating no obvious genetic interaction between *Snx1* and waved-2. Additional crosses with the *Snx2* targeted mutation suggest that both $EGFR^{Wa\text{-}2/Wa\text{-}2}$;$Snx2^{-/-}$ and $EGFR^{Wa\text{-}2/Wa\text{-}2}$;$Snx1^{-/-}$;$Snx2^{+/-}$ mice are recovered in expected frequencies.

DISCUSSION

The generation of targeted null alleles of sorting nexins 1 and 2 demonstrate the two proteins have a highly redundant and necessary function in the mouse. Additionally, $Snx1^{-/-}$; $Snx2^{-/-}$ embryos display a phenotype similar to embryos lacking another retromer homologue, Hβ58 (mouse VPS26). Discovered through an insertional mutagenesis screen, Hβ58 is the only other mammalian retromer homologue to have been mutated in the mouse (Radice *et al.*, 1991; Lee *et al.*, 1992). Both SNX1/SNX2- and Hβ58-deficient embryos exhibit abnormalities beginning at E7.5 and exhibit growth retardation. The mutant embryos develop prominent head folds, a neural axis, heart, and somites. They also fail to grow or differentiate after E10.5, exhibit variability in chorioallantoic fusion, and are in the process of resorption by E11.5. This phenotypic similarity suggests Hβ58 functions in the same genetic pathway as SNX1 and SNX2. *vps5* and *vps26* yeast mutants, which lack the *Saccharomyces cerevisiae* homologues of *Snx1*/*Snx2* and *Hβ58*, demonstrate very similar phenotypes to one another. Just as Vps5p and Vps26p are thought to function together within a single retromer complex, mammalian SNX1/SNX2 and Hβ58 seem to interact and form multimeric protein complexes (Haft *et al.*, 2000). Given these findings, the similarity of the embryonic phenotypes in the mouse strongly argues that SNX1/SNX2 and Hβ58 function within the same mammalian complexes. As a result, these findings provide in vivo evidence for the existence of mammalian complexes that are structurally similar to the yeast retromer and are required for mouse development. Additionally, these genetic studies provide insight into the molecular composition of these complexes. The data indicate that Hβ58 is a required component. Although it has been suggested that SNX1 and SNX2 function together within a single complex, our genetic results reveal that the two proteins can function independently from one another. These findings demonstrate that complexes containing both SNX1 and SNX2 are not essential in the mouse, raising the possibility of two separate but similar complexes.

The trafficking pathway in which SNX1 and SNX2 are involved is not known. Previous studies have suggested that SNX1 and SNX2 function in endosome-to-lysosome trafficking, although the yeast ortholog Vps5p is involved in endosome-to-Golgi trafficking. We identified morphological alterations of apical intracellular compartments within

Snx1$^{-/-}$; *Snx2*$^{-/-}$ visceral endoderm cells by using electron microscopy. This phenotype suggests that cellular trafficking is disrupted in these cells in the absence of SNX1 and SNX2. The identity of the compartments that seem to have accumulated is not clear. In wild-type visceral endoderm cells, apical electron dense compartments are thought to represent a variety of structures associated with the endocytic/lysosomal processes of absorption, degradation, and storage (Jollie, 1990). LysoTracker Red, a fluorescent dye that selectively accumulates in acidic compartments, revealed an altered staining pattern in *Snx1*$^{-/-}$;*Snx2*$^{-/-}$ visceral endoderm cells compared with normal controls. This result suggests that the accumulated compartments seen by electron microscopy may be acidic. Further analysis indicated that these compartments do not seem to be mature lysosomes, because *Snx1*$^{-/-}$;*Snx2*$^{-/-}$ visceral endoderm cells immunostained with LAMP1 and LAMP2 were not distinguishable from control visceral endoderm cells. Furthermore, early endosomes in mutant vs. control visceral endoderm cells, as defined by EEA1 immunostaining, were also indistinguishable. This result is significant because SNX1 and SNX2 have been previously shown to colocalize with EEA1. We can conclude that trafficking defects in *Snx1*$^{-/-}$;*Snx2*$^{-/-}$ visceral endoderm cells are not leading to alterations in the morphology of compartments at the proximal and distal ends of the endosome-to-lysosome pathway

We generated primary embryonic fibroblasts to address whether the abnormalities observed in mutant extraembryonic visceral endoderm cells were represented in embryonic cells. Interestingly, LysoTracker Red did not accumulate in enlarged acidic vesicles in the mutant fibroblasts as it did in the mutant visceral endoderm. This discrepancy may be attributable to the inherent structural and functional differences between polarized visceral endoderm cells and fibroblasts. Conversely, the abnormalities in mutant visceral endoderm cells could be secondary to developmental delay and death of *Snx1*$^{-/-}$;*Snx2*$^{-/-}$ embryos. This latter possibility warrants consideration because wild-type extraembryonic cells failed to rescue *Snx1*$^{-/-}$;*Snx2*$^{-/-}$ embryonic lethality in tetraploid aggregation experiments, suggesting that SNX1 and SNX2 play critical roles in embryonic cells. Embryonic fibroblasts also failed to reveal defects in endocytic trafficking of transferrin and LDL. This result negates the hypothesis that SNX1 and SNX2 are essential for endocytosis in all cells. Embryonic fibroblasts will serve as valuable reagents for further investigation of cellular roles for SNX1 and SNX2 that will potentially elucidate the precise cause of lethality of *Snx1*$^{-/-}$;*Snx2*$^{-/-}$ embryos.

These studies demonstrate that SNX1 and SNX2 are functionally redundant. However, the dramatic evolutionary conservation of SNX1 and SNX2 suggests that the presence and precise function of both proteins provides an evolutionary advantage in both mice and humans (the amino acids of mouse and human SNX1 are ~94% identical, whereas the amino acids of mouse and human SNX2 are ~97% identical). As a result, we expect that in the wild, a SNX1- or SNX2-deficient animal would be at a distinct selective disadvantage in competition with wild-type animals. In fact, we were able to demonstrate phenotypic differences genetically. By reducing the dosage of the paralogous gene in *Snx1*$^{-/-}$ or *Snx2*$^{-/-}$ animals, generating *Snx1*$^{-/-}$;*Snx2*$^{+/-}$ and *Snx1*$^{+/-}$;*Snx2*$^{-/-}$ animals, we show that *Snx1*$^{+/-}$;*Snx2*$^{-/-}$ mice are both runted and under-represented, whereas *Snx1*$^{-/-}$;*Snx2*$^{+/-}$ mice display neither phenotype. These findings demonstrate that the two proteins, or their genetic regulation, are not equivalent. There are many possibilities that could explain these phenotypic differences, including differences in mRNA or protein expression levels, including gross, tissue-specific, or temporal differences. Alternatively, the protein themselves could be functionally unique, differing in protein regulation, membrane specificity, or in cellular cargo transported. There is some evidence that SNX1 and SNX2 may differ in the cellular cargo they might transport. SNX1 and SNX2 have been shown to associate with an overlapping but not identical set of cellular receptors (Haft *et al.*, 1998). If evolutionary divergence has occurred between SNX1 and SNX2 proteins, it is likely to be mediated by the amino terminal portion of the proteins. The first 130 amino acids are less conserved, with roughly 26% identity, whereas the remainder of the proteins, ~390 amino acids, shares ~70% amino acid identity. In the future, a combination of genetic and cellular studies will help elucidate the biology of SNX1, SNX2, and mammalian trafficking complexes that are related to the yeast retromer.

ACKNOWLEDGMENTS

We thank Dr. JoAnn Trejo and Tom Gebuhr for helpful comments on the manuscript. This work was supported with grants from National Institutes of Health (to T.M.).

REFERENCES

Ago, T., Takeya, R., Hiroaki, H., Kuribayashi, F., Ito, T., Kohda, D., and Sumimoto, H. (2001). The PX domain as a novel phosphoinositide-binding module. Biochem. Biophys. Res. Commun. *287*, 733–738.

Bravo, J., *et al*. (2001). The crystal structure of the PX domain from p40(phox) bound to phosphatidylinositol 3-phosphate. Mol. Cell *8*, 829–839.

Cheever, M.L., Sato, T.K., de Beer, T., Kutateladze, T.G., Emr, S.D., and Overduin, M. (2001). Phox domain interaction with PtdIns(3)P targets the Vam7 t-SNARE to vacuole membranes. Nat. Cell Biol. *3*, 613–618.

Chen, B., Bronson, R.T., Klaman, L.D., Hampton, T.G., Wang, J.F., Green, P.J., Magnuson, T., Douglas, P.S., Morgan, J.P., and Neel, B.G. (2000). Mice mutant for EGFR and Shp2 have defective cardiac semilunar valvulogenesis. Nat. Genet. *24*, 296–299.

Cooper, A.A., and Stevens, T.H. (1996). Vps10p cycles between the late-Golgi and prevacuolar compartments in its function as the sorting receptor for multiple yeast vacuolar hydrolases. J. Cell Biol. *133*, 529–541.

Ellson, C.D., *et al*. (2001). PtdIns(3)P regulates the neutrophil oxidase complex by binding to the PX domain of p40(phox). Nat. Cell Biol. *3*, 679–682.

Fowler, K.J., *et al*. (1995). A mutation in the epidermal growth factor receptor in waved-2 mice has a profound effect on receptor biochemistry that results in impaired lactation. Proc. Natl. Acad. Sci. USA *92*, 1465–1469.

Haft, C. R., de la Luz Sierra, M., Bafford, R., Lesniak, M. A., Barr, V. A., and Taylor, S. I. (2000). Human orthologs of yeast vacuolar protein sorting proteins Vps26, 29, and 35: assembly into multimeric complexes. Mol. Biol. Cell *11*, 4105–4116.

Haft, C. R., de la Luz Sierra, M., Barr, V. A., Haft, D. H., and Taylor, S. I. (1998). Identification of a family of sorting nexin molecules and characterization of their association with receptors. Mol. Cell. Biol. *18*, 7278–7287.

Harlow, E., and Lane, D. (1999). Using Antibodies: A Laboratory Manual, Cold Spring Harbor, NY: Cold Spring Harbor Laboratory.

Hogan, B., Beddington, R., Costantini, F., and Lacy, E. (1994). Manipulating the Mouse Embryo: A Laboratory Manual, 2nd ed., Cold Spring Harbor, NY: Cold Spring Harbor Laboratory.

Horazdovsky, B.F., Davies, B.A., Seaman, M.N., McLaughlin, S.A., Yoon, S., and Emr, S.D. (1997). A sorting nexin-1 homologue, Vps5p, forms a complex with Vps17p and is required for recycling the vacuolar protein-sorting receptor. Mol. Biol. Cell *8*, 1529–1541.

Jollie, W.P. (1990). Development, morphology, and function of the yolk-sac placenta of laboratory rodents. Teratology *41*, 361–381.

Kanai, F., Liu, H., Field, S.J., Akbary, H., Matsuo, T., Brown, G.E., Cantley, L.C., and Yaffe, M.B. (2001). The PX domains of p47phox and p40phox bind to lipid products of PI(3)K. Nat. Cell Biol. *3*, 675–678.

Khrebtukova, I., Michaud, E.J., Foster, C.M., Stark, K.L., Garfinkel, D.J., and Woychik, R.P. (1998). Utilization of microhomologous recombination in yeast to generate targeting constructs for mammalian genes. Mutat. Res. *401*, 11–25.

Kurten, R.C., Cadena, D.L., and Gill, G.N. (1996). Enhanced degradation of EGF receptors by a sorting nexin, SNX1. Science *272*, 1008–1010.

Kurten, R.C., Eddington, A.D., Chowdhury, P., Smith, R.D., Davidson, A.D., and Shank, B.B. (2001). Self-assembly and binding of a sorting nexin to sorting endosomes. J. Cell Sci. *114*, 1743–1756.

Lee, J.J., Radice, G., Perkins, C.P., and Costantini, F. (1992). Identification and characterization of a novel, evolutionarily conserved gene disrupted by the murine H beta 58 embryonic lethal transgene insertion. Development *115*, 277–288.

Luetteke, N.C., Phillips, H.K., Qiu, T.H., Copeland, N.G., Earp, H.S., Jenkins, N.A., and Lee, D.C. (1994). The mouse waved-2 phenotype results from a point mutation in the EGF receptor tyrosine kinase. Genes Dev. *8*, 399–413.

Marcusson, E.G., Horazdovsky, B.F., Cereghino, J.L., Gharakhanian, E., and Emr, S.D. (1994). The sorting receptor for yeast vacuolar carboxypeptidase Y is encoded by the VPS10 gene. Cell *77*, 579–586.

Mayor, S., Presley, J.F., and Maxfield, F.R. (1993). Sorting of membrane components from endosomes and subsequent recycling to the cell surface occurs by a bulk flow process. J. Cell Biol. *121*, 1257–1269.

Nagy, A., Gocza, E., Diaz, E.M., Prideaux, V.R., Ivanyi, E., Markkula, M., and Rossant, J. (1990). Embryonic stem cells alone are able to support fetal development in the mouse. Development *110*, 815–821.

Nagy, A., Rossant, J., Nagy, R., Abramow-Newerly, W., and Roder, J.C. (1993). Derivation of completely cell culture-derived mice from early-passage embryonic stem cells. Proc. Natl. Acad. Sci. USA *90*, 8424–8428.

Nakamura, N., Sun-Wada, G.H., Yamamoto, A., Wada, Y., and Futai, M. (2001). Association of mouse sorting nexin 1 with early endosomes. J. Biochem. *130*, 765–771.

Nothwehr, S.F., Bruinsma, P., and Strawn, L.A. (1999). Distinct domains within Vps35p mediate the retrieval of two different cargo proteins from the yeast prevacuolar/endosomal compartment. Mol. Biol. Cell *10*, 875–890.

Nothwehr, S.F., Ha, S.A., and Bruinsma, P. (2000). Sorting of yeast membrane proteins into an endosome-to-Golgi pathway involves direct interaction of their cytosolic domains with Vps35p. J. Cell Biol. *151*, 297–310.

Nothwehr, S.F., and Hindes, A.E. (1997). The yeast VPS5/GRD2 gene encodes a sorting nexin-1-like protein required for localizing membrane proteins to the late Golgi. J. Cell Sci. *110*, 1063–1072.

Ponting, C.P. (1996). Novel domains in NADPH oxidase subunits, sorting nexins, and PtdIns 3-kinases: binding partners of SH3 domains? Protein Sci. *5*, 2353–2357.

Radice, G., Lee, J.J., and Costantini, F. (1991). H beta 58, an insertional mutation affecting early postimplantation development of the mouse embryo. Development *111*, 801–811.

Reddy, J.V., and Seaman, M.N. (2001). Vps26p, a component of retromer, directs the interactions of Vps35p in endosome-to-Golgi retrieval. Mol. Biol. Cell *12*, 3242–3256.

Seaman, M.N., McCaffery, J.M., and Emr, S.D. (1998). A membrane coat complex essential for endosome-to-Golgi retrograde transport in yeast. J. Cell Biol. *142*, 665–681.

Teasdale, R.D., Loci, D., Houghton, F., Karlsson, L., and Gleeson, P.A. (2001). A large family of endosome-localized proteins related to sorting nexin 1. Biochem. J. *358*, 7–16.

Wang, Y., Zhou, Y., Szabo, K., Haft, C.R., and Trejo, J. (2002). Down-regulation of protease-activated receptor-1 is regulated by sorting nexin 1. Mol. Biol. Cell *13*, 1965–1976.

Westphal, V., Marcusson, E.G., Winther, J.R., Emr, S.D., and van den Hazel, H.B. (1996). Multiple pathways for vacuolar sorting of yeast proteinase A. J. Biol. Chem. *271*, 11865–11870.

Xu, Y., Hortsman, H., Seet, L., Wong, S.H., and Hong, W. (2001). SNX3 regulates endosomal function through its PX-domain-mediated interaction with PtdIns(3)P. Nat. Cell Biol. *3*, 658–666.

Zhong, Q., Lazar, C.S., Tronchère, H., Sato, T., Meerloo, T., Yeo, M., Songyang, Z., Emr, S.D., and Gill, G.N. (2002). Endosomal localization and function of sorting nexin 1. Proc. Natl. Acad. Sci. USA *99*, 6767–6772.